

Cite this: *Chem. Sci.*, 2024, 15, 7982

All publication charges for this article have been paid for by the Royal Society of Chemistry

# Structural elucidation of HIV-1 G-quadruplexes in a cellular environment and their ligand binding using responsive <sup>19</sup>F-labeled nucleoside probes†

Sarupa Roy,<sup>a</sup> Priyasha Majee,<sup>b</sup> Sruthi Sudhakar,<sup>b</sup> Satyajit Mishra,<sup>c</sup> Jeet Kalia,<sup>id cd</sup> P. I. Pradeepkumar<sup>id \*b</sup> and Seergazhi G. Srivatsan<sup>id \*a</sup>

Understanding the structure and recognition of highly conserved regulatory segments of the integrated viral DNA genome that forms unique topologies can greatly aid in devising novel therapeutic strategies to counter chronic infections. In this study, we configured a probe system using highly environment-sensitive nucleoside analogs, 5-fluoro-2'-deoxyuridine (FdU) and 5-fluorobenzofuran-2'-deoxyuridine (FBFdU), to investigate the structural polymorphism of HIV-1 long terminal repeat (LTR) G-quadruplexes (GQs) by fluorescence and <sup>19</sup>F NMR. FdU and FBFdU, serving as hairpin and GQ sensors, produced distinct spectral signatures for different GQ topologies adopted by LTR G-rich oligonucleotides. Importantly, systematic <sup>19</sup>F NMR analysis in *Xenopus laevis* oocytes gave unprecedented information on the structure adopted by the LTR G-rich region in the cellular environment. The results indicate that it forms a unique GQ-hairpin hybrid architecture, a potent hotspot for selective targeting. Furthermore, structural models generated using MD simulations provided insights on how the probe system senses different GQs. Using the responsiveness of the probes and *Taq* DNA polymerase stop assay, we monitored GQ- and hairpin-specific ligand interactions and their synergistic inhibitory effect on the replication process. Our findings suggest that targeting GQ and hairpin motifs simultaneously using bimodal ligands could be a new strategy to selectively block the viral replication.

Received 15th March 2024  
Accepted 23rd April 2024

DOI: 10.1039/d4sc01755b

rsc.li/chemical-science

## Introduction

HIV-1 is one of the most lethal retroviruses, which induces a chronic infection by etching the host cell genome with a proviral DNA that is reverse transcribed from its RNA genome. Established treatments use a cocktail of drugs having different modes of action to control the disease progression.<sup>1</sup> However, due to persistence of latent reservoirs, drug-resistance and promiscuity of the viral polymerase, it is very hard to eradicate the virus completely from the host system.<sup>2,3</sup> One of the current ways to counter latency involves awakening dormant viruses

and simultaneously inhibiting viral replication with antiviral agents.<sup>4,5</sup> It is also hypothesized that targeting certain structural and functional segments of the integrated viral DNA genome could complement the above strategy and help in curing the disease.<sup>6</sup> An important and a highly conserved gene segment that could be suitable for this purpose is the long terminal repeat (LTR) of the HIV-1 promoter region.<sup>7,8</sup>

The initiation of HIV-1 transcription is navigated by the promoter region 5'-LTR, which is composed of U3, R and U5 regions.<sup>9</sup> The U3 region consists of three functional segments including the highly conserved core-binding site of NF-κB and Sp1 transcription factors,<sup>10</sup> which harbors contiguous G-rich tracts capable of forming G-quadruplex (GQ) structures namely LTR-II, LTR-III and LTR-IV, and HIVpro1 and HIVpro2 (Fig. 1A).<sup>11-13</sup> Notably, LTR-III and LTR-IV form GQs *in vitro* in a mutually exclusive manner. While LTR-III adopts a unique architecture made of a hybrid-type GQ juxtaposed with a three G-C paired hairpin motif, LTR-IV attains a parallel GQ topology with a T-bulge (Fig. 1B).<sup>14,15</sup> However, the entire G-rich region majorly forms the GQ-hairpin form like the LTR-III motif, and the parallel form of LTR-IV is induced when it binds to ligands or protein factors.<sup>14-16</sup> Importantly, the LTR GQ region represents an evolutionary conserved element across all primate lentiviruses, and the balance between different GQ structures is implicated in the propagation and latency of the virus.<sup>17,18</sup>

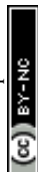
<sup>a</sup>Department of Chemistry, Indian Institute of Science Education and Research (IISER), Pune, Dr Homi Bhabha Road, Pune 411008, India. E-mail: srivatsan@iiserpune.ac.in

<sup>b</sup>Department of Chemistry, Indian Institute of Technology Bombay, Mumbai 400076, India. E-mail: pradeep@chem.iitb.ac.in

<sup>c</sup>Department of Biological Sciences, Indian Institute of Science Education and Research (IISER) Bhopal, Bhopal Bypass Road, Bhauri, Bhopal 462066, India

<sup>d</sup>Department of Chemistry, Indian Institute of Science Education and Research (IISER) Bhopal, Bhopal Bypass Road, Bhauri, Bhopal 462066, India

† Electronic supplementary information (ESI) available: Experimental details, CD, T<sub>m</sub>, fluorescence, MD simulation, mass, NMR spectra and gel images. Experimental procedure for NMR measurements of ONs in a cellular environment, and ligand interaction with LTR GQs and their effects on the *Taq* DNA polymerase activity are described. See DOI: <https://doi.org/10.1039/d4sc01755b>



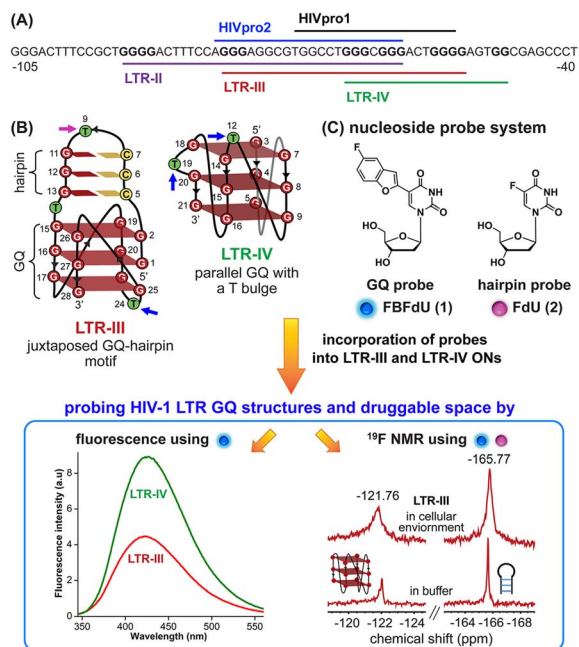


**Fig. 1** (A) Schematic representation of the HIV-1 LTR G-rich region. (B) Secondary structures of LTR-III and LTR-IV GQs are depicted using the respective NMR structures (PDB: 6H1K and 2N4Y). (C) Environment-sensitive nucleoside probe system designed to probe the structural polymorphism and druggable space of LTR GQs by fluorescence and  $^{19}\text{F}$  NMR techniques in cell-free and cellular environments. Potential sites for incorporation of the GQ probe (FBFdU 1) and hairpin probe (FdU 2) into the loop region of LTR-III and LTR-IV G-rich sequences are shown with blue and magenta arrows, respectively.

Therefore, we envision that the virus status can be selectively controlled in the host cell by using structure-specific binders. In this direction, it is important to gain a comprehensive understanding of the structural polymorphism, dynamics and druggable space of LTR GQs in a cellular environment to advocate a viable therapeutic strategy.

A multitude of biophysical and biochemical techniques including CD, UV thermal melting, fluorescence, NMR and X-ray crystallography add pieces of valuable information to characterize GQs *in vitro*.<sup>19–25</sup> Recently, antibodies and chemical probes have been developed to detect ensembles of DNA GQs in cells.<sup>26–30</sup> However, the majority of tools fall short when evaluating co-existing structures, as the challenges are twofold: (i) inability to differentiate different GQ topologies (exceptions are few)<sup>31–34</sup> and (ii) limited capability to assess structures in a cellular environment. Also, sequences with multiple G tracts exhibit high structural polymorphism and dynamics, which can vary between cell-free and cellular environments.<sup>35,36</sup> Therefore, we sought to devise a probe platform that would (i) provide spectral signatures for different GQs formed by the LTR G-rich region, which could help identify the preferred GQ in cells and (ii) allow us to survey the chemical space of LTR GQs to design structure-specific binders.

In this context, we developed microenvironment-sensitive dual-functional nucleoside probes that immensely aid in studying nucleic acid conformations and topology-specific ligand/drug interaction.<sup>37,38</sup> In particular, 5-fluorobenzofuran-

modified 2'-deoxyuridine (FBFdU) serves as an excellent two-channel readout system to detect different GQ conformations of the human telomeric repeat *in vitro* and in cellular milieu by using fluorescence and  $^{19}\text{F}$  NMR techniques.<sup>37</sup> However, LTR-III forms a juxtaposed GQ-hairpin motif that is unique for the HIV-1 virus. Hence, we realized that by using only a GQ sensing probe (FBFdU) it would not be possible to survey the landscape of the LTR. In this regard, here we report the development of a probe system that uses FBFdU as a GQ sensor and 5-fluoro-2'-deoxyuridine (FdU) as a hairpin sensor (Fig. 1C). The probes judiciously placed in loop positions of the LTR G-rich region are minimally perturbing, and importantly, produce distinct and resolved spectral signatures for LTR-III and LTR-IV GQs. Rewardingly, we deduced the GQ structure adopted by the LTR promoter region in an *ex vivo* model (*Xenopus laevis* oocyte extract) by using  $^{19}\text{F}$  NMR signatures obtained *in vitro*. Furthermore, the probe platform and *Taq* DNA polymerase assay helped in mapping ligand interactions and their influence on the LTR replication process.

## Results and discussion

### Structural investigation of the modified HIV-1 LTR by fluorescence and $^{19}\text{F}$ NMR *in vitro*

**Design of the nucleoside probe platform.** The loop orientation, composition and loop residue interaction with neighboring bases are very different amongst the GQs.<sup>39,40</sup> Environment-sensitive nucleoside analogs capable of sensing these differences act as good GQ probes.<sup>41,42</sup> Therefore, to configure a probe system, we decided to exploit the differences in the structural features of LTR GQs, particularly at the loop nucleoside level. A 28-mer ON 3 representing the LTR-III region adopts a parallel-antiparallel hybrid-type GQ structure comprising three stacked tetrads connected by four loops (Fig. 1B and Table 1).<sup>14</sup> The 12-nucleotide diagonal loop (3–14 residues) forms a juxtaposed hairpin motif wherein three G–C base pairs are capped by a loop formed by G<sub>8</sub>–T<sub>9</sub>–G<sub>10</sub> residues. We envisioned that T<sub>9</sub>, part of the hairpin loop and T<sub>24</sub>, part of a 3-nt lateral loop (A<sub>22</sub>–C<sub>23</sub>–T<sub>24</sub>) connecting the G-tetrads would be potential sites for placing nucleoside probes to distinguish hairpin and GQ motifs. On the other hand, LTR-IV ON 8 adopts an all-parallel stranded GQ with a T<sub>19</sub> bulge that stacks with A<sub>17</sub> of the propeller loop (Fig. 1B and Table 1). It is shown that T<sub>19</sub> is not mandatory for GQ formation, and hence, placing a GQ sensor at this position should not affect the native GQ structure. Furthermore, a 4-nt propeller loop formed by A<sub>10</sub>–C<sub>11</sub>–T<sub>12</sub>–G<sub>13</sub> bases is also envisioned as a good location to place the probe.<sup>15</sup> Based on this key information, we used a combination of two highly conformation-sensitive nucleoside probes, FBFdU (GQ sensor)<sup>37</sup> and FdU (hairpin/duplex sensor),<sup>43,44</sup> to distinguish different structures adopted by the LTR G-rich region (Fig. 1B and C). A foreseeable advantage of this probe combination is that the chemical shift region of FBFdU (around –122 ppm) and FdU (around –165 ppm) is significantly different so that the individual domains can be unequivocally distinguished, which otherwise is difficult by other currently available tools (*vide infra*).



Table 1 Sequence of native and modified LTR ONS

G-rich domain	ON <sup>a</sup>	5'—3'
LTR-III	3	GGGAGGCGTGGCCTGGGCGGGACTGGGG
	4	GGGAGGCG2GGCCTGGGCGGGAC1GGGG
	5	GGGAGGCGTGGCCTGGGCGGGAC1GGGG
	6	GGGAGGCG2GGCCTGGGCGGGACTGGGG
	7	CCCCAGTCCCGCCAGGCCACGCCTCCC
LTR-IV	8	CTGGGCGGGACTGGGGAGTGGT
	9	CTGGGCGGGAC1GGGGAGTGGT
	10	CTGGGCGGGACTGGGGAG1GGT
	11	ACCACTCCCGAGTCCCGCCAG
LTR-III + IV	12	AGGGAGGCGTGGCCTGGGCGGGACTGGGGAGTGGT
	13	AGGGAGGCGTGGCCTGGGCGGGAC1GGGGAGTGGT
	14	AGGGAGGCGTGGCCTGGGCGGGACTGGGGAG1GGT
	15	AGGGAGGCG2GGCCTGGGCGGGACTGGGGAGTGGT
	16	AGGGAGGCG2GGCCTGGGCGGGACTGGGGAG1GGT

<sup>a</sup> ONS 3, 8 and 12 are native unmodified ONS of LTR-III, LTR-IV and LTR-(III + IV), respectively. ONS 4–6 are native LTR-III modified with FBFdU (1) and or FdU (2) at T<sub>24</sub> and T<sub>9</sub>, respectively. ONS 9 and 10 are native LTR-IV modified with FBFdU (1) at T<sub>12</sub> and T<sub>19</sub>, respectively. ONS 13–16 are native LTR-(III + IV) modified with FBFdU (1) and or FdU (2) at T<sub>25</sub> or T<sub>32</sub> and T<sub>10</sub>, respectively. 7 and 11 are complementary ONS of 3 and 8, respectively.

**LTR-III GQ-hairpin motif.** Based on the structural considerations, ON 4 was synthesized wherein FBFdU was incorporated at the GQ domain (T<sub>24</sub>) and FdU was incorporated at the hairpin domain (T<sub>9</sub>) using phosphoramidites 1a and 2a, respectively (Scheme S1†). The ON was purified by gel electrophoresis and characterized by mass analysis (Fig. S1 and S2, Table S1†). CD spectra of control unmodified ON 3 and modified ON 4 were found to be similar depicting the formation of a hybrid GQ topology with positive bands at ~265 nm and ~285 nm (Fig. S3A†).<sup>14</sup> The GQ form of ON 4 exhibited a slightly higher *T<sub>m</sub>* value as compared to the native ON 3 (Fig. S3B and Table S2†). These results indicate that the incorporation of FBFdU and FdU has only a minor impact on the formation and stability of the ON 4 GQ structure.

The ability of FBFdU to serve as a GQ reporter was evaluated by recording fluorescence of LTR-III ON 4 and its corresponding duplex (4·7) in a buffer containing K<sup>+</sup> ions (Fig. 2A and B). The GQ form of 4 displayed a discernibly lower fluorescence intensity and a slightly red-shifted emission band (417 nm) as compared to its perfect duplex (4·7, 414 nm). In support of our probe system design, the <sup>19</sup>F NMR spectrum of ON 4 exhibited two distinct peaks at -122.51 ppm and -165.73 ppm arising from FBFdU and FdU, respectively (Fig. 2C, blue line). <sup>1</sup>H NMR spectra of ON 4 and 3 revealed imino proton signals for both GQ and hairpin domains (Fig. S4†). To assign signals in the <sup>19</sup>F NMR spectrum, two singly modified ONS 5, containing FBFdU at T<sub>24</sub> (GQ domain) and 6, containing FdU at T<sub>9</sub> (hairpin domain), were synthesized (Table 1, Fig. 2A, S1 and S2†). CD profiles and *T<sub>m</sub>* values indicated the formation of a stable hybrid GQ structure like the native 3 and modified 4 ONS

(Fig. S3A and B, Table S2†). While ON 5 produced a single peak at -122.51 ppm from the GQ sensor (Fig. 2C, red line), ON 6 gave a signal at -165.71 ppm from the hairpin sensor similar to ON 4 (Fig. 2C, green line). Hence, signals emanating from FBFdU (-122.51 ppm) and FdU (-165.73 ppm) of ON 4 are assigned to GQ and hairpin domains, respectively. When ON 4 was annealed to its complementary ON 7, the duplex structure produced new peaks at -121.54 ppm associated with FBFdU and -165.62 ppm associated with FdU (Fig. S5†). <sup>1</sup>H NMR also validated the formation of a duplex structure where characteristic peaks for Watson-Crick H-bonded imino protons appeared between 12 and 14 ppm, with no peaks in the GQ region (Fig. S5†). Henceforth, the probe system provides a simplified <sup>19</sup>F NMR spectrum to detect the two domains of LTR-III ON 4 simultaneously.

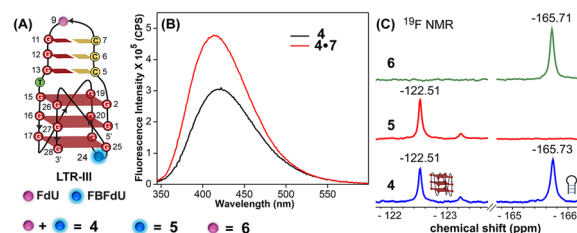


Fig. 2 (A) Schematic representation of the juxtaposed GQ-hairpin structure of LTR-III. ON 4 is modified with FdU at T<sub>9</sub> and FBFdU at T<sub>24</sub> positions. ON 5 contains FBFdU at the T<sub>24</sub> position. ON 6 contains FdU at the T<sub>9</sub> position. (B) Fluorescence spectra of ON 4 (GQ) and its duplex 4·7. The samples were excited at 330 nm with excitation and emission slit widths of 7 nm and 9 nm, respectively. (C) <sup>19</sup>F NMR spectra of ONS 4–6.



**LTR-IV GQs.** Next, we studied the LTR-IV G-rich region by incorporating FBFdU at  $T_{12}$  (ON **9**) and  $T_{19}$  (ON **10**) positions using the modified phosphoramidite **1a** (Table 1 and Fig. S3A†) and the purity and identity of ONs were ascertained by HPLC and mass analysis (Fig. S1, S2 and Table S1††). According to our presumption, FBFdU placed at these positions did not affect the formation and stability of the native parallel GQ topology as deduced by CD and UV-thermal melting experiments (Fig. S3C and D, Table S2†). ONs **9** and **10** reported the formation of a GQ structure with an intense emission band centered at around 428 nm (Fig. 3B). However, the corresponding duplexes showed reduced emission. In particular, duplex **10**·**11** displayed a significant reduction in fluorescence intensity. Notably,  $^{19}\text{F}$  NMR spectra of ON **9** ( $75\ \mu\text{M}$ ) exhibited multiple peaks revealing the formation of different GQ structures (Fig. 3C, blue line). Imino proton signals appearing between 10 and 12 ppm supported the formation of GQs (Fig. S6†). GQs can stack on top of each other by 5'-5' end-to-end stacking interaction resulting in higher order GQs, and such structures are usually observed for sequences capable of forming a parallel topology.<sup>45</sup> Hence, in consensus with the literature,<sup>15</sup> the observed  $^{19}\text{F}$  signals could be associated with higher order structures originating from the monomeric parallel GQ motif. To further evaluate the  $^{19}\text{F}$  signals, NMR spectra of ON **9** were recorded at a much lower concentration (favors monomeric form) and in the presence of a synthetic crowding agent (*e.g.*, PEG, favors higher-ordered structures).<sup>46</sup>  $^{19}\text{F}$  NMR recorded at a lower concentration of the ON **9** ( $10\ \mu\text{M}$ ) produced a major peak at  $-120.42\ \text{ppm}$ , which was also present at a higher concentration of the ON (Fig. 3C, purple line). While this peak was assigned to the monomeric GQ structure, a peak at  $-121.74\ \text{ppm}$  in PEG 200 (40% v/v) is likely due to the formation of a higher-ordered GQ structure (green line). The formation of GQ structures under these conditions was further confirmed by  $^1\text{H}$  NMR (Fig. S6†). ON **9** hybridized to its complementary ON **11** exhibited a single  $^{19}\text{F}$  peak for the duplex form, which was also ascertained by  $^1\text{H}$  NMR (Fig. 3C, red line and Fig. S6†). Although ON **10** containing the modification at the  $T_{19}$  position exhibited multiple  $^{19}\text{F}$  peaks, the spectrum was not well resolved (Fig. S7†). Peak broadening was also observed in the  $^1\text{H}$  NMR spectrum, and

hence, this sequence was not used in further studies. Taken together, these results endorse that FBFdU is a useful GQ tool that allows access to study sequences forming multiple structures.

### Probing the GQ structure of the LTR in a physiological environment by NMR

The LTR G-rich promoter region encompassing both LTR-III and IV segments was recently characterized by Richter and Phan groups *in vitro* using  $^1\text{H}$  NMR. Their results suggest that it largely forms a juxtaposed GQ-hairpin motif like LTR-III.<sup>14</sup> As an important step forward, we decided to use the spectral properties of our nucleoside analogs to systematically determine the GQ structure adopted by the LTR region in a cellular environment and probe its druggable space. In-cell  $^{19}\text{F}$  NMR has become a powerful tool to study nucleic acid structures in cellular milieu,<sup>37,47–49</sup> as fluorine is 100% abundant, highly sensitive and importantly, absent in cellular systems (no background signal).<sup>50–55</sup> Furthermore, its signal does not undergo significant line broadening in the heterogeneous cellular environment, which is very severe in the case of a proton signal.<sup>56</sup> To determine  $^{19}\text{F}$  signatures of the longer LTR region and survey GQ and hairpin structures, ONs **13–15** labeled with FBFdU in the GQ domain or FdU in the hairpin domain were synthesized (Table 1, Fig. 4A, S1 and S2†). Importantly, the modification position was maintained as in the individual LTR G-rich segments. CD spectra of modified (**13–15**) and control unmodified (**12**) ONs exhibited bands similar to the hybrid topology adopted by the LTR-III region (Fig. S8A†). While ON **13** (FBFdU at  $T_{25}$ ) displayed a nearly  $4\ ^\circ\text{C}$  higher  $T_m$  compared to the native ON **12**, ON **14** (FBFdU at  $T_{32}$ ) and **15** (FdU at  $T_{10}$ ) displayed similar  $T_m$  values (Fig. S8B and Table S2†). ON **13** showed a single broad  $^{19}\text{F}$  peak at  $-123.20\ \text{ppm}$  and ON **14** exhibited a sharper peak at  $-122.10\ \text{ppm}$  for the GQ domain (Fig. 4B). ON **15** produced a distinct peak ( $-165.72\ \text{ppm}$ ) for the hairpin domain.  $^1\text{H}$  NMR spectra of ONs clearly revealed the presence of imino protons for GQ and hairpin motifs (Fig. 4B). Furthermore, the absence of multiple  $^{19}\text{F}$  peaks suggests that the parallel topology of the LTR-IV region is possibly not formed by the longer promoter region (compare with Fig. 3C). To detect both GQ and hairpin motifs simultaneously, we synthesized ON

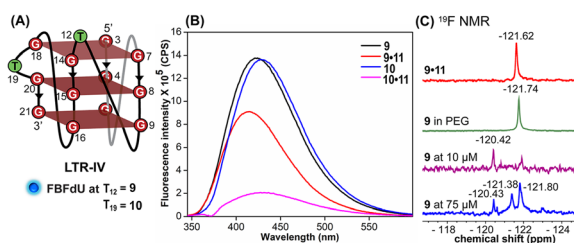


**Fig. 3** FBFdU reports the formation of LTR-IV GQs. (A) Schematic representation of the parallel GQ structure of LTR-IV ON. ON **9** contains FBFdU at the  $T_{12}$  position. ON **10** contains FBFdU at the  $T_{19}$  position. **9**·**11** and **10**·**11** are corresponding duplexes. (B) Fluorescence spectra ( $1\ \mu\text{M}$ ) of ONs **9** and **10** (GQ) and their duplexes. The samples were excited at  $330\ \text{nm}$  with excitation and emission slit widths of  $6\ \text{nm}$  and  $7\ \text{nm}$ , respectively. (C)  $^{19}\text{F}$  NMR spectra of ON **9** under different conditions.

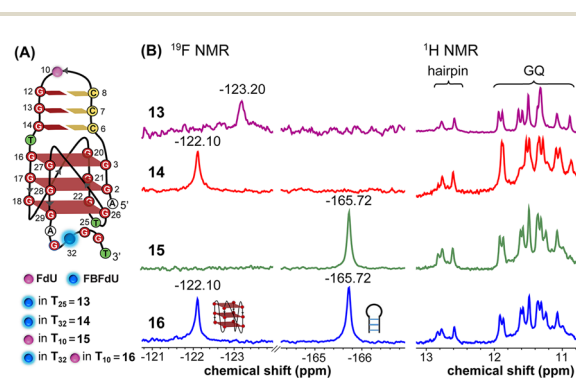


**Fig. 4** (A) Schematic representation of the juxtaposed GQ-hairpin structure of the LTR-III + IV region. (B)  $^{19}\text{F}$  NMR and partial  $^1\text{H}$  NMR spectra of ONs **13–16**.



16 containing FdU at T<sub>10</sub> and FBFdU at T<sub>32</sub> positions. Modification at T<sub>25</sub> (like in ON 13) was avoided as it led to a broader peak and poor base line.

Rewardingly, ON 16 displayed two distinct signals, one each for GQ (−122.10 ppm) and hairpin (−165.72 ppm) structures with the same chemical shifts as that of ONs 14 and 15 designed to detect the structures independently (Fig. 4B). Also, ON 16 depicted a <sup>1</sup>H NMR spectrum revealing the presence of GQ and hairpin structures. Collectively, the probe combination provides distinct and simplified <sup>19</sup>F signatures for GQ and hairpin structures, and our results demonstrate that the LTR G-rich region predominantly folds into a GQ-hairpin motif similar to LTR-III *in vitro*.

To obtain a progressive understanding of the LTR GQs in cell-free and cellular environments, we performed a systematic NMR analysis using *Xenopus* oocytes, a commonly used cellular model.<sup>47–49,57</sup> While a buffer mimicking intraocyte (IO) ionic conditions serves as a cell-free system, frog egg lysate and extract serve as very good *ex vivo* systems to carry out NMR experiments to determine the structure of nucleic acids. First, we recorded the <sup>19</sup>F NMR spectrum of ON 16 in an IO buffer (25 mM HEPES pH 7.5, 110 mM KCl, 10.5 mM NaCl, 130 nM CaCl<sub>2</sub>, 1 mM MgCl<sub>2</sub>, 0.1 mM EDTA). The ON acquired a conformation like LTR-III, reflecting peaks at −122.02 ppm for the GQ and −165.65 ppm for the hairpin motifs (Fig. 5, blue line and Fig. S9†). The formation of the GQ-hairpin structure was confirmed by <sup>1</sup>H NMR and CD experiments (Fig. 5 and S10†). ON 16 incubated in the lysate supported the formation of a hybrid architecture like in the IO buffer (Fig. 5, red line). The inter-phase egg extract obtained by simply centrifuging crushed eggs maintains metabolite and protein contents mimicking those in the biological environment.<sup>46</sup> Interestingly, the <sup>19</sup>F NMR spectrum of ON 16 incubated in the egg extract revealed the presence of GQ and hairpin motifs, albeit with a slight broadening and shift in the signal (green line). In contrast, due to extensive line broadening, the <sup>1</sup>H NMR spectrum fails to provide structural information in egg extract (Fig. 5).<sup>46,57</sup> Therefore, our fluorine-labeled nucleoside probes outweigh the applicability of proton NMR in cell-based analysis. To confirm if the signal is originating from the intact ON in cellular samples,

after NMR acquisition, the samples were analyzed by HPLC and ESI-MS. The results indicated that the ON is not degraded in the cellular environment (Fig. S11 and S12†). Taken together, these results provide clear evidence for the presence of a monomeric architecture preserving juxtaposed GQ and hairpin domains both *in vitro* and under cellular conditions underscoring the potential of LTR GQ as a target of selective therapeutic intervention.

**Computational models provide insights on how the probe system senses LTR GQs.** Fluorescence of FBFdU is enhanced and red-shifted in a polar environment but quenched by stacking interaction and the electron transfer process with an adjacent guanosine base (Table S3†).<sup>37,58</sup> Also, the orientation of the FBF ring relative to uracil impacts its fluorescence intensity. Therefore, observed differences in fluorescence intensity of GQ and duplex structures are due to differences in the microenvironment around the probe. To examine the probe environment and its interaction with neighboring bases, structural models of labeled LTR-III ON 4 and LTR-IV ONs 9 and 10 were generated. Force field parameters of FdU and FBFdU (Fig. S13 and S14†) were first calculated and were incorporated into the templates with PDB ID: 6H1K and 2N4Y.<sup>14,15</sup> Two control systems, LTR-III ON 3 and LTR-IV ON 8, were also generated. The root mean square deviation (RMSD) revealed that MD simulations are well equilibrated (Fig. S15†). Superimposition of the major cluster of ON 4 and the native ON 3 is almost identical (Fig. S16 and Fig. S17A†). In ON 4, FBFdU placed at T<sub>24</sub> strongly stacks below the tetrad formed by G<sub>25</sub>·G<sub>28</sub>·G<sub>17</sub>·G<sub>21</sub> and experiences a hydrophobic environment (Fig. 6A–C). The plots representing the center of mass (COM) distance and angle defined between the normal to FBFdU and G<sub>28</sub> showed steady values of ~5 Å and 0–45° (~82% stacking), respectively, which are the defined parameters for proper stacking interaction (Fig. S18†).<sup>59</sup> This major conformation exists for ~86% of the simulation, which manifests in the form of a low intense band around an emission maximum of methanol (417 nm, Fig. 2B). In the case of duplex 4–7, C5-modified FBFdU flanked between C<sub>23</sub> and G<sub>25</sub> would be projected in the major groove and is likely to experience less stacking interaction as compared to in the GQ structure. Hence,

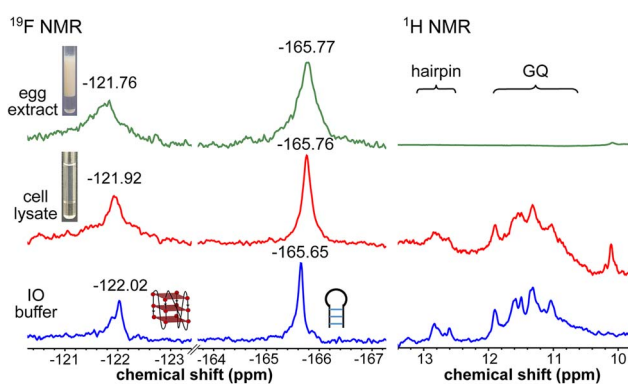


Fig. 5 LTR region forms a GQ-hairpin structure in a cellular environment as detected using FBFdU and FdU. <sup>19</sup>F and <sup>1</sup>H NMR spectra of ON 16 (100 μM) in IO buffer, frog egg lysate and extract (*ex vivo* cell model).

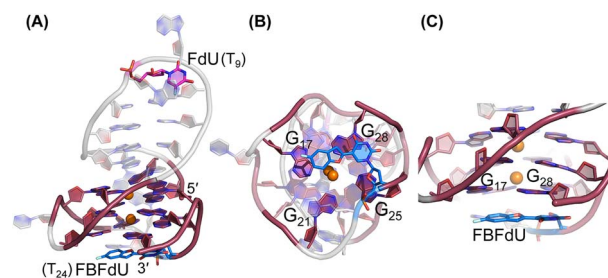


Fig. 6 Representative images of major clusters of LTR-III ON 4. (A) Overall structure with FdU and FBFdU in ON 4. (B) Axial view showing the stacking of FBFdU over the bottom quartet. (C) Zoomed-in image showing the perpendicular orientation of FBFdU stacked with G<sub>17</sub> and G<sub>28</sub>. GQ bases are represented in maroon, FdU in magenta and FBFdU in blue. K<sup>+</sup> ions are represented as orange spheres. The clusters have been obtained from the 500 ns MD simulation. Details of MD simulations are provided in the ESI.†



the duplex displays higher fluorescence intensity with no apparent change in the emission maximum. A similar conformation has been observed for C5-heterocycle-modified pyrimidine nucleoside analogs in duplexes.<sup>60,61</sup>

Simulations of LTR-IV ON **9** revealed 3 clusters of ~30, 30, and 26% each, and ON **10** revealed 2 clusters accounting for ~85% of the population (Fig. S19 and S20†). The modified base adopts an alternate conformation without affecting the GQ topology (Fig. S21 and S22†). Models of **9** and **10** revealed that the probe placed at T<sub>12</sub> and T<sub>19</sub> positions, respectively, is flipped out (solvent exposed) and is away from the G-tetrad core (Fig. S21 and S22†). Hence, these ONs exhibit high fluorescence intensity with emission maxima similar to the emission wavelength of the nucleoside analog **1** in water, indicating a polar environment around the probe (423 nm and 428 nm, Table S3†). In the case of duplex **9**·**11**, FBFdU flanked between C<sub>11</sub> and G<sub>13</sub> would experience partial stacking interaction, and hence, shows lower fluorescence intensity at λ<sub>em</sub> = 418 nm. FBFdU in duplex **10**·**11** exhibits significant reduction in fluorescence intensity due to partial stacking interaction followed by more quenching from two adjacent Gs (G<sub>18</sub> and G<sub>20</sub>). Although the <sup>19</sup>F component of nucleoside probes exhibits distinct chemical shifts for different GQ and duplex structures, rationalizing peak positions is not trivial. This is because the environment around the probes and their interaction with neighbouring bases as mentioned above can have varying shielding-desielding effects on the <sup>19</sup>F atom,<sup>62–64</sup> which are difficult to predict and are also evident from an obscure trend in the chemical shift of nucleosides in different solvents (Table S4†).

### Probing ligand binding to HIV-1 LTR GQs by fluorescence, <sup>19</sup>F NMR and *Taq* DNA polymerase stop assay

Using the spectral properties of the probes, we evaluated ligand recognition of LTR ONs using two structurally different GQ binders namely, TMPyP4 and BRACO19 (Fig. S23A†). Upon ligand binding to the GQ structure, the fluorescence of FBFdU placed in the GQ domain is known to diminish significantly because of its proximity to the polyaromatic ligands.<sup>37</sup> LTR-III ON **4** was titrated with increasing concentrations of the ligands and changes in fluorescence were recorded. Titration with TMPyP4 and BRACO19 resulted in a dose-dependent quenching in fluorescence intensity with minimum changes in the emission maximum (Fig. S24A and B†). A plot of normalized fluorescence intensity *versus* ligand concentration fitted to the Hill equation gave an apparent *K*<sub>d</sub> value of 0.28 ± 0.05 μM and 0.56 ± 0.09 μM, respectively (Fig. S23B†). Similarly the parallel GQ structure of LTR-IV ON **9** titrated with the ligands gave *K*<sub>d</sub> values of 0.33 ± 0.02 μM and 0.39 ± 0.05 μM, respectively (Fig. S23C, S25A and B†). The <sup>19</sup>F label of FBFdU efficiently reported the formation of different GQ-ligand complexes with distinct chemical shifts. TMPyP4 and BRACO19 binding to the GQ domain of LTR-III ON **4** produced a new peak at -120.75 ppm and -120.78 ppm, respectively, with a concomitant decrease in the GQ signal (Fig. S23D and S24C†). Gratifyingly, as these ligands bind preferentially to the G-tetrad, they did not exhibit detectable interaction with the

hairpin structure. This is evident from the chemical shift of FdU (-165.73 ppm), placed in the hairpin domain, which remains mostly unchanged throughout the titration experiment. Similarly, ligand binding to the parallel topology of LTR-IV ON **9** exhibited a distinct peak for each complex (TMPyP4: -120.77 ppm and BRACO19: -120.60 ppm, Fig. S23E and S25C†). Interestingly, upon ligand binding, multiple GQs formed by **9** coalesce into one ligand-bound form.

Bioinformatics and biophysical studies reveal the prevalence of quadruplex-hairpin/duplex junctions in genomes, characterized by varying loop sizes and conformations.<sup>65–69</sup> These adjacently placed structures offer unique scaffolds to target the junction or both GQ and duplex elements simultaneously.<sup>70–72</sup> Hence, bimodal ligands capable of doing the same can significantly enhance the specific targeting of hybrid GQs as opposed to autonomous GQ structures. In this direction, we evaluated the recognition properties of the GQ-hairpin motif of the longer LTR promoter ON **16** using TMPyP4 (GQ binder) and doxorubicin (DOX, duplex binder) by fluorescence and <sup>19</sup>F NMR (Fig. S26A†). Addition of increasing concentrations of TMPyP4 (30 nM–2.5 μM) to ON **16** (0.5 μM) resulted in a progressive quenching in fluorescence intensity as before and gave an apparent *K*<sub>d</sub> value of 0.52 ± 0.03 μM for the formation of the ligand-GQ complex (Fig. S26B and S27A†). Preferential binding of the ligand to the GQ region was ascertained by <sup>19</sup>F NMR. FBFdU placed at the GQ domain responded to increasing concentrations of the ligand, giving rise to a new peak at -120.69 ppm for the complex (Fig. 7A). Notably, the chemical shift of FdU (-165.72 ppm) placed in the hairpin domain remained practically unaltered, indicating that TMPyP4 interacts specifically with the GQ structure.

DOX is intrinsically fluorescent and it shows changes in fluorescence upon binding to DNA. To avoid interference from FBFdU, DOX (2 μM) was titrated with a control unmodified ON **12** (2.5 nM–2 μM). We observed a sigmoidal quenching behavior, which gave a *K*<sub>d</sub> value of 0.10 ± 0.02 μM (Fig. S26B and S27B†). <sup>19</sup>F NMR using ON **16** gave better insights into the recognition process. Addition of DOX (1 equiv.) to the ON resulted in the emergence of two new peaks—(i) -120.79 ppm associated with GQ-DOX and (ii) -165.98 ppm associated with hairpin-DOX (Fig. 7B). Notably, at a higher equivalent of DOX, the ligand largely occupies the hairpin domain and to some

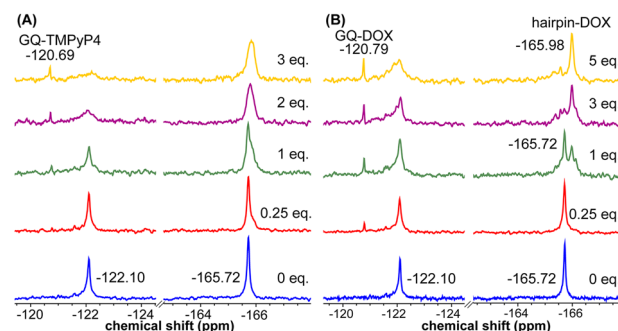


Fig. 7 FBFdU and FdU report structure-specific ligand binding to the LTR GQ-hairpin structure. (A) and (B) <sup>19</sup>F NMR spectra of ON **16** as a function of increasing TMPyP4 and DOX concentration, respectively.



extent the GQ domain. These results highlight the advantage of  $^{19}\text{F}$ -labeled nucleoside analogs in probing structure-specific ligand interactions. Based on these observations, we designed a polymerase stop assay to study the inhibitory effect of the GQ structure and the ligands independently and in a combination.

The effect of GQ structures on DNA polymerase activity was evaluated by *Taq* DNA polymerase stop assay using a native LTR template **T1** encompassing III and IV regions and a mutated template **T2** (does not fold into a GQ, Fig. 8A and Table S5†). GQ forming template **T1** significantly halted the polymerization process yielding largely stalled products near the GQ site (Fig. S28,† lanes 2–6, 8B). Longer reaction times (30 min) produced only ~33% of the full-length product. In contrast, reactions in the presence of a non-GQ forming template **T2** produced significant amounts of the full-length product in only 2 min (~45%), which progressively increased to ~80% at 30 min (Fig. S28,† lanes 7–11, 8B). These observations indicate that the stalling of the primer extension reaction is due to the formation of a stable LTR GQ structure by **T1**.

Next, we studied the effect of ligand binding to the GQ structure on the polymerase activity using **T1** (Fig. 8C). For this purpose, a reaction time of 20 min was chosen as it gave reasonable amounts of the full-length product (~25%, Fig. S28,† lane 5). Varying concentrations of TMPyP4 and DOX were independently added and allowed to bind with LTR GQ, and then primer extension reactions were carried out as before. Upon addition of TMPyP4 there was a noticeable decrease in the formation of the full-length product, accompanied by a simultaneous increase in stalled products (Fig. S29,† lanes 2–5, Fig. 8D). At 0.75  $\mu\text{M}$  of the ligand (7.5 equiv. w.r.t **T1**) no

detectable full-length product was observed (Fig. S29,† lane 6). Similarly, increasing amounts of DOX resulted in a progressive reduction in the formation of the full-length product (Fig. S29,† lane 7–10, Fig. 8D). Although DOX inhibited the polymerase activity, it required a higher amount (20 equiv.) to produce an effect comparable to TMPyP4 (Fig. S29,† compare lane 6 and 10). This may be due to DOX competing for the primer-template duplex, hairpin and GQ regions. These results prompted us to study the combined effect of ligands, wherein different concentrations of TMPyP4 and DOX at a 1 : 1 ratio were added to the reaction mixture. The gel image revealed a synergistic effect of ligands as the formation of the full-length product considerably decreased with a concomitant increase in truncated products in comparison to reactions in which only one ligand was added at an equivalent concentration (Fig. 8D, S29,† lanes 11–14). The effect is noticeable when we compare TMPyP4 (0.3  $\mu\text{M}$ , ~16%), DOX (1  $\mu\text{M}$ , ~17%), and TMPyP4+DOX (0.3  $\mu\text{M}$ , ~9%, Fig. 8D). These results suggest that the GQ-hairpin motif of the LTR G-rich region serves as a highly conserved regulatory element to potentially block the viral replication process by targeting both GQ and hairpin domains simultaneously.

Based on our results and the formation of a unique GQ-hairpin architecture in a cellular environment, we propose that bimodal ligand scaffolds composed of GQ and duplex binders, clamped using an appropriate linker, could selectively target the HIV-1 LTR and profoundly attenuate its pathogenesis (Fig. S30†). Needless to say, careful consideration should be exercised when optimizing the ligand design. The choice of GQ and hairpin binders from available examples and linker length, flexibility and point of attachment to the ligands will be very crucial.

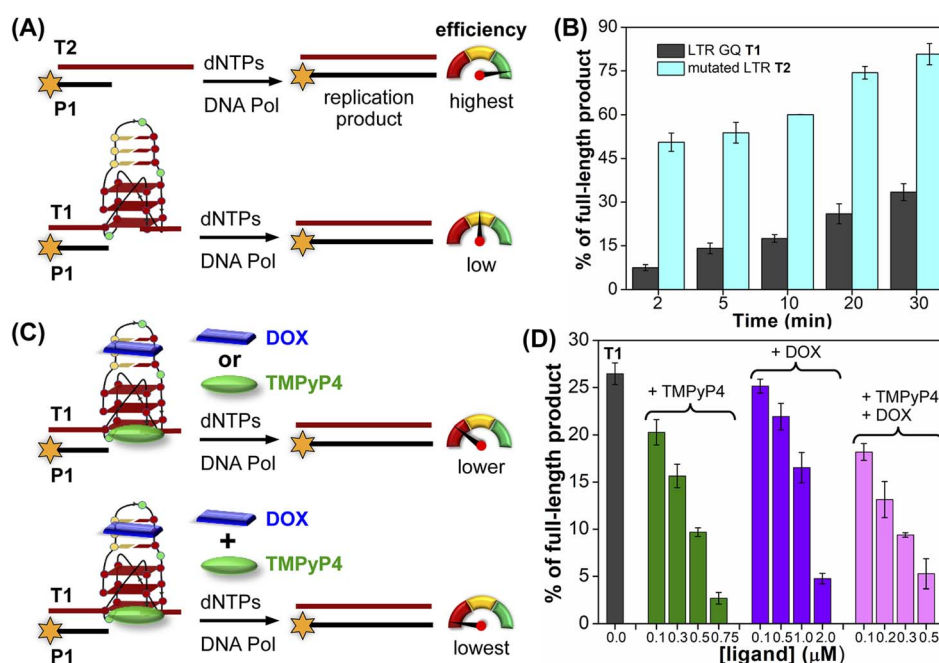


Fig. 8 Schematic representation of primer extension reactions using *Taq* DNA polymerase (A) with non-GQ forming template **T2** and GQ forming template **T1**, (C) in the presence of ligands TMPyP4 or DOX and TMPyP4 + DOX. (B) and (D) Percentage of the full-length product obtained from *Taq* DNA polymerase reactions. (B) Reactions performed using templates **T1** and **T2** at different time intervals. (D) Reactions performed using **T1** with increasing concentrations of ligands TMPyP4, DOX and TMPyP4 + DOX at 20 min. For gel images, see Fig. S28 and S29.† Values are denoted as mean  $\pm$  s.d. for 2 independent experiments.



## Conclusion

We have devised a probe platform using two highly environment-sensitive nucleoside analogs (FBFdU and FdU) to study the structural polymorphism of a conserved HIV-1 LTR G-rich region in cell-free and cellular environments. These minimally invasive analogs produced a very simplified spectrum with distinct fluorescence and  $^{19}\text{F}$  NMR signatures for different LTR GQ architectures. Importantly, using  $^{19}\text{F}$  signatures of FBFdU and FdU we successfully identified that the LTR G-rich region adopts a GQ-hairpin architecture in a cellular environment. MD simulations gave insights on the structural basis by which FBFdU fluorescently senses different GQ topologies and distinguishes them from the duplex form. Furthermore, the nucleoside probes facilitated the detection and estimation of structure-specific ligand interactions by fluorescence and  $^{19}\text{F}$  NMR techniques. Polymerase stop assay confirmed the regulatory function of LTR GQ structures. While TMPyP4 (GQ binder) and DOX (duplex binder) individually decreased polymerase activity, an equimolar mixture exhibited a synergistic inhibitory effect on LTR replication. Taken together, these findings suggest that simultaneous targeting of the juxtaposed GQ-hairpin motif using bimodal ligands could be a rational plan to selectively and efficiently inhibit the pathogenesis of the virus. In this direction, the FBFdU and FdU combination offers a versatile platform to study the structure as well as devise screening assays to identify hybrid ligands targeting GQ-hairpin/duplex motifs.

## Data availability

The datasets supporting this article have been uploaded as part of the ESI.† Deposited MD simulation models are available in <https://www.modelarchive.org/>. Details are provided in the ESI (Fig. S16, S19 and S20).†

## Author contributions

S. G. S. designed and supervised this project. S. R. designed and performed the experiments. P. M., S. S. and P. I. P. performed MD simulations to build models of labeled GQ structures. S. M. and J. K. helped in performing experiments in frog egg lysate and extract. All authors analysed the results, and S. R. and S. G. S. wrote the manuscript in consultation with all the authors.

## Conflicts of interest

There are no conflicts to declare.

## Acknowledgements

S. R. and S. M. acknowledge CSIR, India, for their graduate research fellowships. P. M. thanks IIT Bombay and S. S. thanks Prime Ministers Research Fellowship (PMRF) for graduate research fellowships. We thank Spacetime-IIT Bombay for HPC facilities. This work was supported by SERB (CRG/2022/000284) grant to S. G. S and IIT Bombay-Institute of Eminence (IOE) funds to P. I. P.

## References

- 1 Y. Peng, Y. Zong, D. Wang, J. Chen, Z.-S. Chen, F. Peng and Z. Liu, *Front. Pharmacol.*, 2023, **26**, 1294966.
- 2 R. J. Pomerantz, *Clin. Infect. Dis.*, 2002, **34**, 91–97.
- 3 R. K. Gupta, J. Gregson, N. Parkin, H. Haile-Selassie, A. Tanuri, F. L. Andrade, P. Kaleebu, C. Watera, A. Aghokeng, N. Mutenda, J. Dzungare, S. Hone, Z. Z. Hang, J. Garcia, Z. Garcia, P. Marchorro, E. Beteta, A. Giron, R. Hamers, S. Inzaule, L. M. Frenkel, M. H. Chung, T. de Oliveira, D. Pillay, K. Naidoo, A. Kharsany, R. Kugathasan, T. Cutino, G. Hunt, S. A. Rios, M. Doherty, M. R. Jordan and S. Bertagnolio, *Lancet Infect. Dis.*, 2018, **18**, 346–355.
- 4 A. Archin, L. Liberty, A. D. Kashuba, S. K. Choudhary, J. D. Kuruc, A. M. Crooks, D. C. Parker, E. M. Anderson, M. F. Kearney, M. C. Strain, D. D. Richman, M. G. Hudgens, R. J. Bosch, J. M. Coffin, J. J. Eron, D. J. Hazuda and D. M. Margolis, *Nature*, 2012, **487**, 482–485.
- 5 W. Nguyen, J. Jacobson, K. E. Jarman, H. Jousset Sabroux, L. Harty, J. McMahon, S. R. Lewin, D. F. Purcell and B. E. Sleeb, *J. Med. Chem.*, 2019, **62**, 5148–5175.
- 6 J. Zhang and C. Crumpacker, *Viruses*, 2022, **14**, 1084.
- 7 K. A. Roebuck and M. Saifuddin, *Gene Expression*, 1999, **8**, 67–84.
- 8 T. van Opijnen, R. E. Jeeninga, M. C. Boerlijst, G. P. Pollakis, V. Zetterberg, M. Salminen and B. Berkhout, *J. Virol.*, 2004, **78**, 3675–3683.
- 9 L. A. Pereira, K. Bentley, A. Peeters, M. J. Churchill and N. J. Deacon, *Nucleic Acids Res.*, 2000, **28**, 663–668.
- 10 R. E. Jeeninga, M. Hoogenkamp, M. Armand-Ugon, M. de Baar, K. Verhoef and B. Berkhout, *J. Virol.*, 2000, **74**, 3740–3751.
- 11 R. Perrone, M. Nadai, I. Frasson, J. A. Poe, E. Butovskaya, T. E. Smithgall, M. Palumbo, G. Palu and S. N. Richter, *J. Med. Chem.*, 2013, **56**, 6521–6530.
- 12 S. Amrane, A. Kerkour, A. Bedrat, B. Vialet, M.-L. Andreola and J.-L. Mergny, *J. Am. Chem. Soc.*, 2014, **136**, 5249–5252.
- 13 A. De Rache, J. Marquevielle, S. Bouaziz, B. Vialet, M. L. Andreola, J.-L. Mergny and S. Amrane, *J. Mol. Biol.*, 2023, **436**, 168359.
- 14 E. Butovskaya, B. Heddi, B. Bakalar, S. N. Richter and A. T. Phan, *J. Am. Chem. Soc.*, 2018, **140**, 13654–13662.
- 15 B. De Nicola, C. J. Lech, B. Heddi, S. Regmi, I. Frasson, R. Perrone, S. N. Richter and A. T. Phan, *Nucleic Acids Res.*, 2016, **44**, 6442–6451.
- 16 E. Ruggiero, I. Frasson, E. Tosoni, M. Scalabrin, R. Perrone, M. Marušič, J. Plavec and S. N. Richter, *ACS Infect. Dis.*, 2022, **8**, 958–968.
- 17 Y. Sheng, B. Cao, M. X. Ou, Y. Wang, S. M. Yuan, N. Zhang, T. Zou and Y. Liu, *Chem. Commun.*, 2021, **57**, 5298–5301.
- 18 R. Perrone, E. Lavezzo, G. Palù and S. N. Richter, *Sci. Rep.*, 2017, **7**, 2018.
- 19 M. Vorlíčková, I. Kejnovská, J. Sagi, D. Renčíuk, K. Bednářová, J. Motlová and J. Kypr, *Methods*, 2012, **57**, 64–75.





- 20 R. A. Darby, M. Sollogoub, C. McKeen, L. Brown, A. Risitano, N. Brown, C. Barton, T. Brown and K. R. Fox, *Nucleic Acids Res.*, 2002, **30**, e39.
- 21 B. R. Vummidi, J. Alzeer and N. W. Luedtke, *ChemBioChem*, 2013, **14**, 540–558.
- 22 J. Mohanty, N. Barooah, V. Dhamodharan, S. Harikrishna, P. I Pradeepkumar and A. C. Bhasikuttan, *J. Am. Chem. Soc.*, 2013, **135**, 367–376.
- 23 D. Sun and L. H. Hurley, *Methods Mol. Biol.*, 2010, **608**, 65–79.
- 24 S. M. Haider, G. N. Parkinson and S. Neidle, *J. Mol. Biol.*, 2003, **326**, 117–125.
- 25 T. Santos, G. F. Salgado, E. J. Cabrita and C. S. Cruz, *Pharmaceuticals*, 2021, **14**, 769.
- 26 G. Biffi, D. Tannahill, J. McCafferty and S. Balasubramanian, *Nat. Chem.*, 2013, **5**, 182–186.
- 27 A. Henderson, Y. Wu, Y. C. Huang, E. A. Chavez, J. Platt, F. B. Johnson, R. M. Brosh Jr, D. Sen and P. M. Lansdrop, *Nucleic Acids Res.*, 2014, **42**, 860–869.
- 28 S. Galli, L. Melidis, S. M. Flynn, D. Varshney, A. Simeone, J. Spiegel, S. K. Madden, D. Tannahill and S. Balasubramanian, *J. Am. Chem. Soc.*, 2022, **144**, 23096–23103.
- 29 F. Doria, M. Nadai, M. Zuffo, R. Perrone, M. Freccero and S. N. Richter, *Chem. Commun.*, 2017, **53**, 2268–2271.
- 30 J. Robinson, S. G. Stenspil, K. Maleckaite, M. Bartlett, M. D. Antonio, R. Vilar and M. K. Kuimova, *J. Am. Chem. Soc.*, 2024, **146**, 1009–1018.
- 31 J.-H. Yuan, W. Shao, S.-B. Chen, Z.-S. Huang and J.-H. Tan, *Biochem. Biophys. Res. Commun.*, 2020, **531**, 18–24.
- 32 T. Vo, S. Oxenford, R. Angell, C. Marchetti, S. A. Ohnmacht, W. D. Wilson and S. Neidle, *ACS Med. Chem. Lett.*, 2020, **11**, 991–999.
- 33 S. Kumar, S. P. P. Pany, S. Sudhakar, S. B. Singh, C. S. Todankar and P. I. Pradeepkumar, *Biochemistry*, 2022, **61**, 2546–2559.
- 34 S. Takahashi, A. Kotar, H. Tateishi-Karimata, S. Bhowmik, Z. F. Wang, T. C. Chang, S. Sato, S. Takenaka, J. Plavec and N. Sugimoto, *J. Am. Chem. Soc.*, 2021, **143**, 16458–16469.
- 35 R. Rigo, E. Groaz and C. Sissi, *Pharmaceuticals*, 2022, **15**, 373.
- 36 J. T. Grün and H. Schwalbe, *Biopolymers*, 2022, **113**, e23477.
- 37 S. Manna, D. Sarkar and S. G. Srivatsan, *J. Am. Chem. Soc.*, 2018, **140**, 12622–12633.
- 38 A. Nuthanakanti, I. Ahmed, S. Y. Khatik, K. Saikrishnan and S. G. Srivatsan, *Nucleic Acids Res.*, 2019, **47**, 6059–6072.
- 39 M. Cheng, Yu. Cheng, J. Hao, G. Jia, J. Zhou, J.-L. Mergny and C. Li, *Nucleic Acids Res.*, 2018, **46**, 9264–9275.
- 40 J. Jana, Y. M. Vianney, N. Schröder and K. Weisz, *Nucleic Acids Res.*, 2022, **50**, 7161–7175.
- 41 M. Sproviero, K. L. Fadock, A. A. Witham and R. A. Manderville, *ACS Chem. Biol.*, 2015, **10**, 1311–1318.
- 42 S. Manna and S. G. Srivatsan, *RSC Adv.*, 2018, **8**, 25673–25694.
- 43 M. Olejniczak, Z. Gdaniec, A. Fischer, T. Grabarkiewicz, L. Bielecki and R. W. Adamiak, *Nucleic Acids Res.*, 2002, **30**, 4241–4249.
- 44 K. Tanabe, M. Sugiura and S. Nishimoto, *Bioorg. Med. Chem.*, 2010, **18**, 6690–6694.
- 45 N. Q. Do and A. T. Phan, *Chem.–Eur. J.*, 2012, **18**, 14752–14759.
- 46 R. Hänsel, F. Löhr, S. Foldynová-Trantírková, E. Bamberg, L. Trantírek and V. Dötsch, *Nucleic Acids Res.*, 2011, **39**, 5768–5775.
- 47 H.-L. Bao, T. Ishizuka, T. Sakamoto, K. Fujimoto, T. Uechi, N. Kenmochi and Y. Xu, *Nucleic Acids Res.*, 2017, **45**, 5501–5511.
- 48 H.-L. Bao, T. Masuzawa, T. Oyoshi and Y. Xu, *Nucleic Acids Res.*, 2020, **48**, 7041–7051.
- 49 C. Wang, G. Xu, X. Liu, L. Jiang, X. Zhou, M. Liu and C. Li, *J. Am. Chem. Soc.*, 2024, **146**, 4741–4751.
- 50 H. Chen, S. Viel, F. Ziarelli and L. Peng, *Chem. Soc. Rev.*, 2013, **42**, 7971–7982.
- 51 D. Gimenez, A. Phelan, C. D. Murphy and S. L. Cobb, *Beilstein J. Org. Chem.*, 2021, **17**, 293–318.
- 52 K. Fauster, C. Kreutz and R. Micura, *Angew. Chem., Int. Ed.*, 2012, **51**, 13080–13084.
- 53 M. R. Baranowski, M. Warminski, J. Jemielity and J. Kowalska, *Nucleic Acids Res.*, 2020, **48**, 8209–8224.
- 54 Q. Li, M. Trajkovski, C. Fan, J. Chen, Y. Zhou, K. Lu, H. Li, X. Su, Z. Xi, J. Plavec and C. Zhou, *Angew. Chem., Int. Ed.*, 2022, **61**, e2022018.
- 55 M. Wang, M. Lu, M. P. Fritz, C. M. Quinn, I. L. Byeon, C.-H. Byeon, J. Struppe, W. Maas, A. M. Gronenborn and T. Polenova, *Angew. Chem., Int. Ed.*, 2018, **57**, 16375–16379.
- 56 L. B. T. Pham, A. Costantino, L. Barbieri, V. Calderone, E. Luchinat and L. Banci, *J. Am. Chem. Soc.*, 2023, **145**, 1389–1399.
- 57 R. Hänsel, S. Foldynová-Trantírková, F. Löhr, J. Buck, E. Bongartz, E. Bamberg, H. Schwalbe, V. Dötsch and L. Trantírek, *J. Am. Chem. Soc.*, 2009, **131**, 15761–15768.
- 58 S. Doose, H. Neuweiler and M. Sauer, *ChemPhysChem*, 2009, **10**, 1389–1398.
- 59 H. S. Hayatshahi, N. M. Henriksen and T. E. Cheatham, *J. Chem. Theory Comput.*, 2018, **14**, 1456–1470.
- 60 N. J. Greco and Y. Tor, *J. Am. Chem. Soc.*, 2005, **127**, 10784–10785.
- 61 J. Riedl, R. Pohl, L. Rulišek and M. Hocek, *J. Org. Chem.*, 2012, **77**, 1026–1044.
- 62 H. Sapper and W. Lohmann, *Biophys. Struct. Mech.*, 1978, **4**, 327–335.
- 63 C. S. Giam and J. L. Lyle, *J. Am. Chem. Soc.*, 1973, **95**, 3235–3239.
- 64 J. N. Dahanayake, C. Kasireddy, J. P. Karnes, R. Verma, R. M. Steinert, D. Hildebrandt, O. A. Hull, J. M. Ellis and K. R. Mitchell-Koch, *Annu. Rep. NMR Spectrosc.*, 2018, **93**, 281–365.
- 65 Y. M. Vianney and K. Weisz, *Nucleic Acids Res.*, 2022, **50**, 11948–11964.
- 66 M. L. Greco, A. Kotar, R. Rigo, C. Cristofari, J. Plavec and C. Sissi, *Nucleic Acids Res.*, 2017, **45**, 10132–10142.
- 67 M. Yang, S. Carter, S. Parmar, D. D. Bume, D. R. Calabrese, X. Liang, K. Yazdani, M. Xu, Z. Liu, C. J. Thiele and J. S. Schneekloth, *Nucleic Acids Res.*, 2021, **49**, 7856–7869.



- 68 S. Y. Khatik, S. Sudhakar, S. Mishra, J. Kalia, P. I. Pradeepkumar and S. G. Srivatsan, *Chem. Sci.*, 2023, **14**, 5627–5637.
- 69 R. K. R. Sannapureddi, M. K. Mohanty, L. Salmon and B. Sathyamoorthy, *J. Am. Chem. Soc.*, 2023, **145**, 15370–15380.
- 70 L. Díaz-Casado, I. Serrano-Chacón, L. Montalvillo-Jiménez, F. Corzana, A. Bastida, A. G. Santana, C. González and J. L. Asensio, *Chem.–Eur. J.*, 2021, **27**, 6204–6212.
- 71 T. Q. N. Nguyen, K. W. Lim and A. T. Phan, *Sci. Rep.*, 2017, **7**, 11969.
- 72 S. Mandal, Y. Kawamoto, Z. Yue, K. Hashiya, Y. Cui, T. Bando, S. Pandey, M. E. Hoque, M. A. Hossain, H. Sugiyama and H. Mao, *Nucleic Acids Res.*, 2019, **47**, 3295–3305.

